

Supporting Information

Prussian blue anode for high performance electrochemical deionization promoted by faradic mechanism

Lu Guo^{1*}, Runwei Mo^{1*}, Wenhui Shi¹, Zhi Yi Leong¹, Meng Ding¹, Fuming Chen¹ and Hui Ying Yang^{1*}

¹ Pillar of Engineering Product Development, Singapore University of Technology and Design, 8 Somapah Road, 487372, Singapore.

*Corresponding author. Tel.: +65 6303 6663; Fax: +65 6779 5161. E-mail address: yanghuiying@sutd.edu.sg (H. Y. Yang).

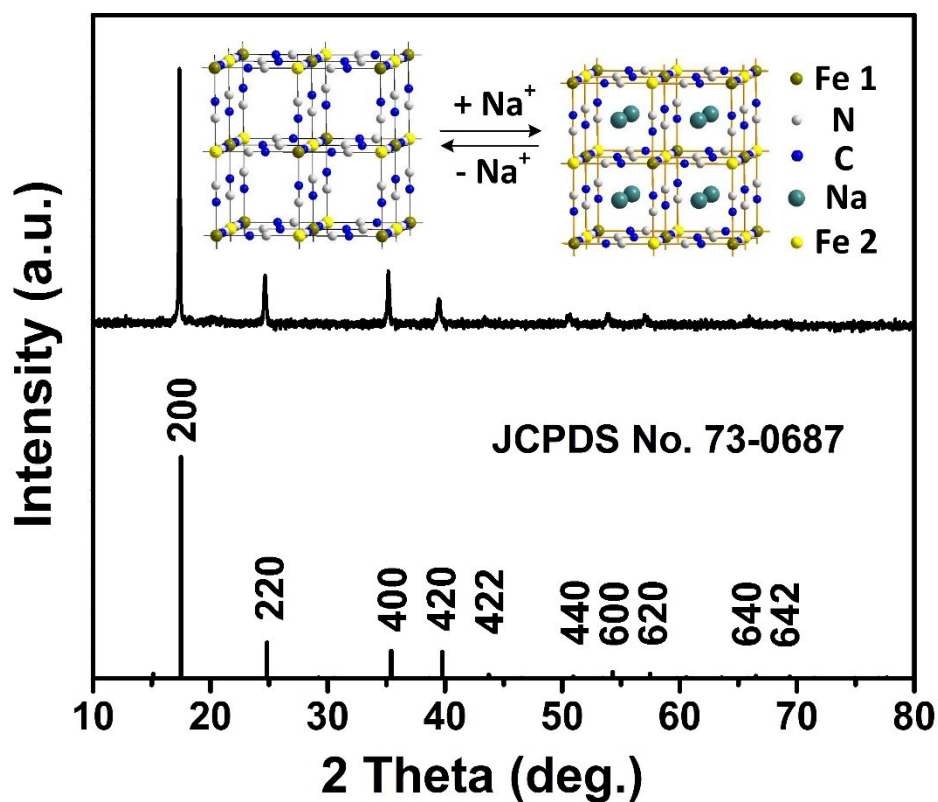


Figure S1. XRD pattern of PB, the inserts illustrate the lattice structures of Prussian blue before and after sodium insertion.

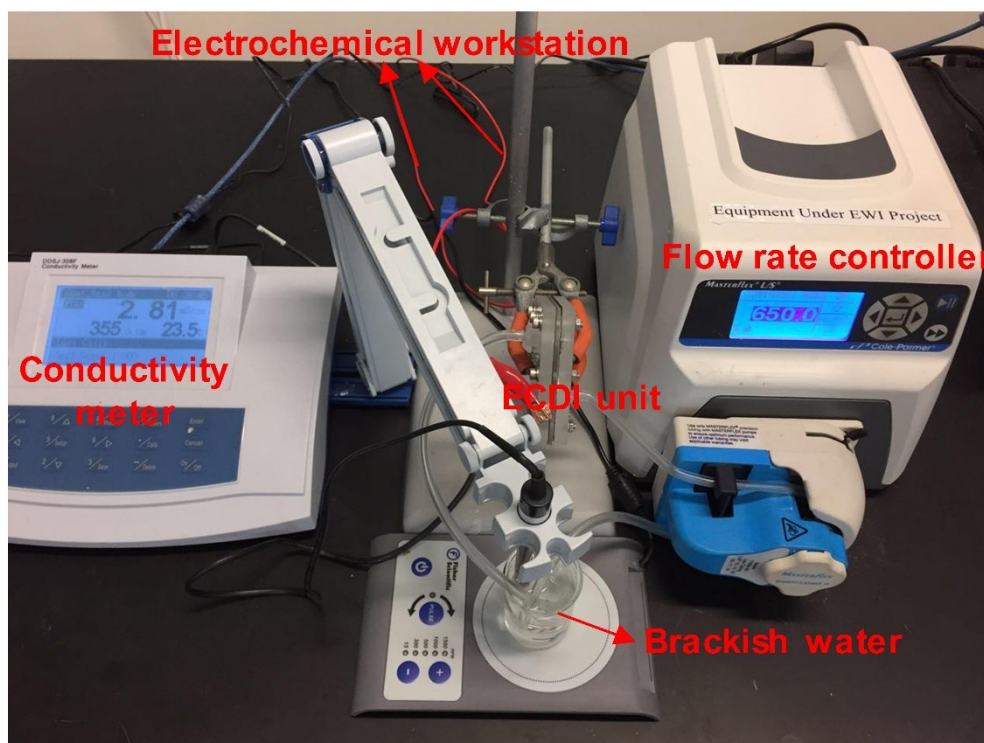


Figure S2. Photograph of the flow through system for electrochemical deionization.

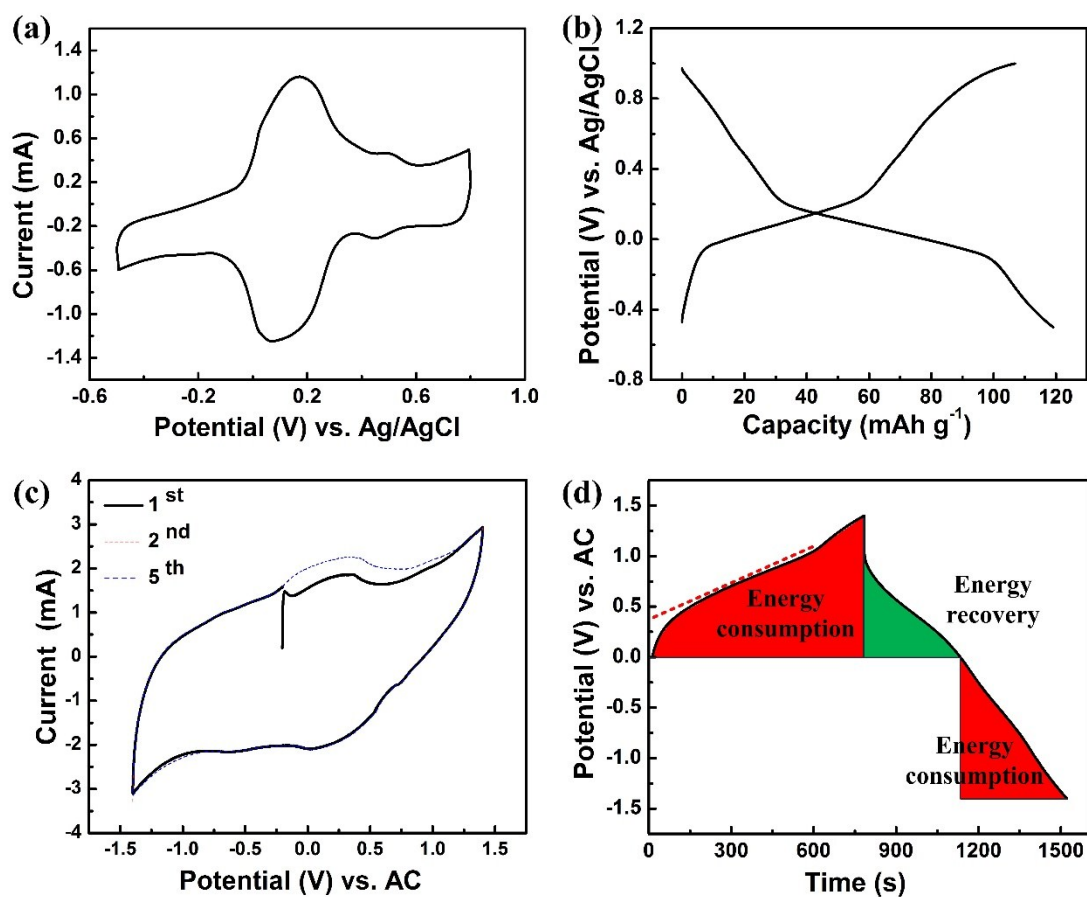


Figure S3. (a) CV curve in a three-electrode system at a scan rate of 1 mV s⁻¹ in 1 M sodium chloride solution. (b) Charge and discharge profile of Prussian blue electrode in a three-electrode system with a current density of 250 mA g⁻¹ in 1 M sodium chloride solution. (c) CV curves of the Prussian blue electrode measured at a scan rate of 1 mV s⁻¹ within a flow through system shown in fig S2. (d) A typical charging and discharging curve of EDI within a flow through system at 1 C (125 mA g⁻¹) with the plateau during first charging process highlighted. The red and green colours represent energy consumed and recovered respectively in the EDI. The total energy consumption should be calculated by total energy consumption = energy consumption – energy recovery.

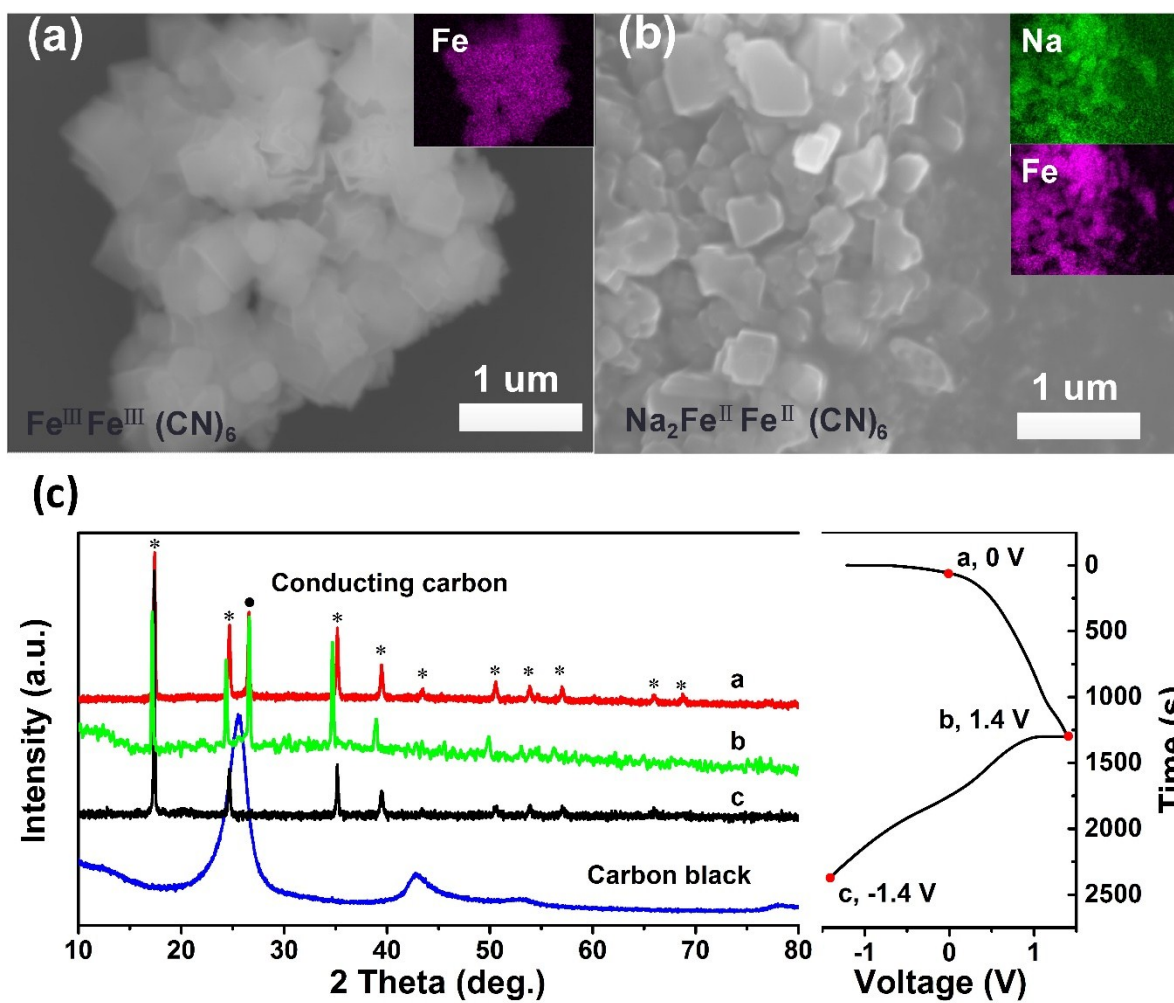


Figure S4. SEM images and element mapping images of Prussian blue before (a) and after (b) 100 cycles. (c) A charge/ discharge curve of the deionization process and changes of the XRD patterns at different voltages.

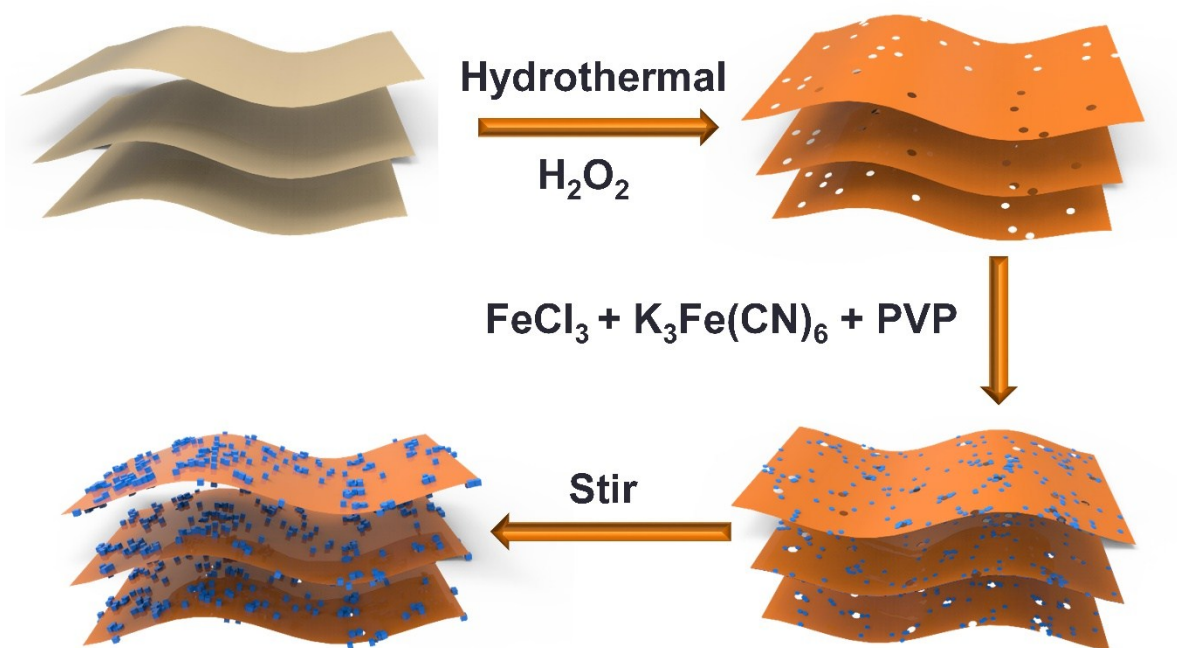


Figure S5. Schematic diagram of the synthesis process of PB@NPG.

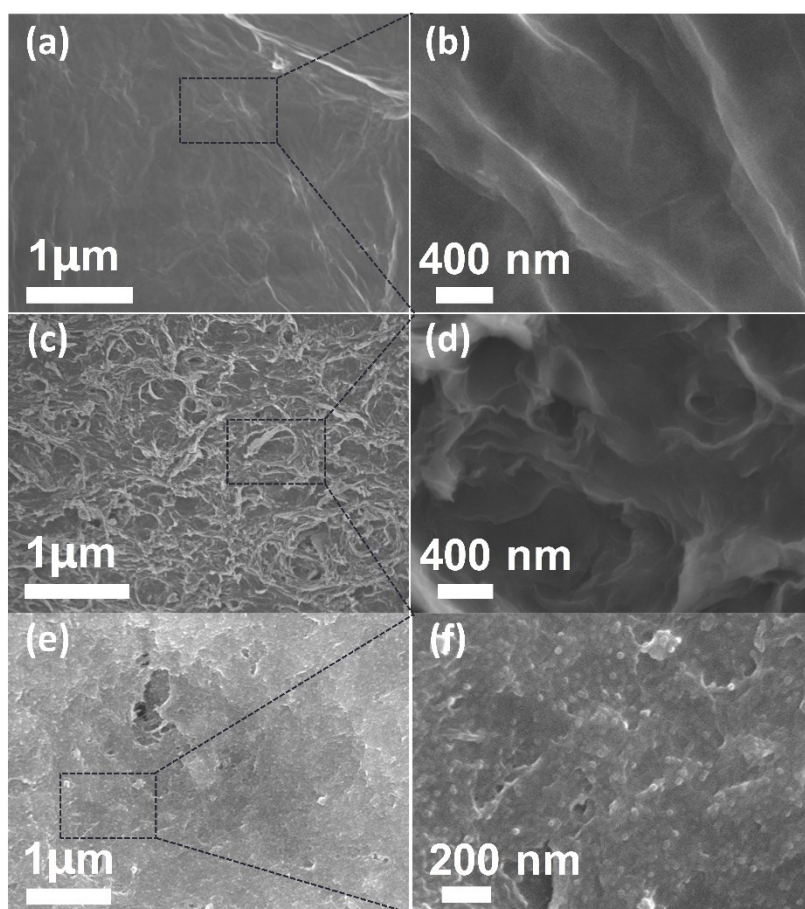


Figure S6. The SEM images of rGO (a, b), NPG (c, d) and PB@NPG (e, f), respectively.

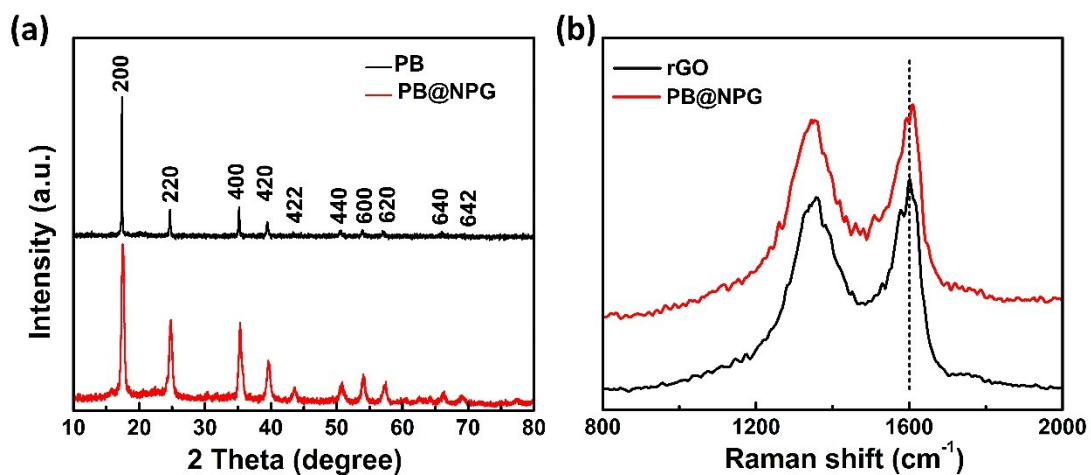


Figure S7. The XRD patterns (a) and Raman Spectra (b) of PB and PB@NPG respectively, the intensity ratios of D band to G band (I_D/I_G) for rGO and PB@NPG are 0.9 and 1.0 respectively.

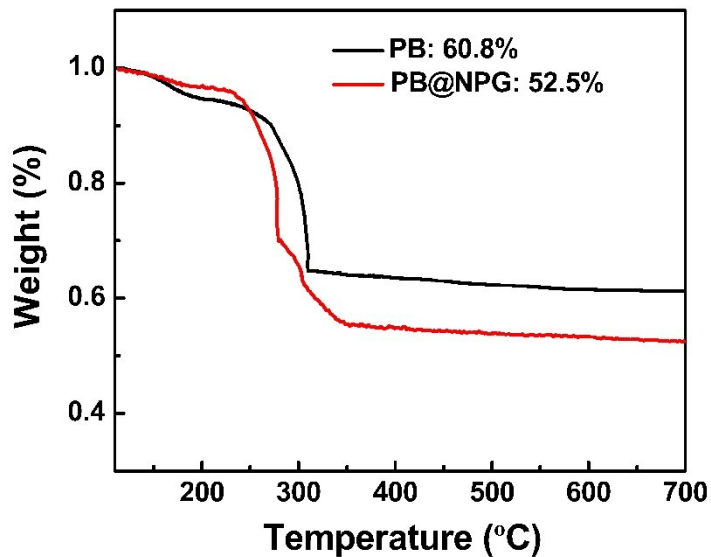


Figure S8. TGA profiles of PB and PB@NPG measured at a heating rate of $5\text{ }^\circ\text{C min}^{-1}$ in air.

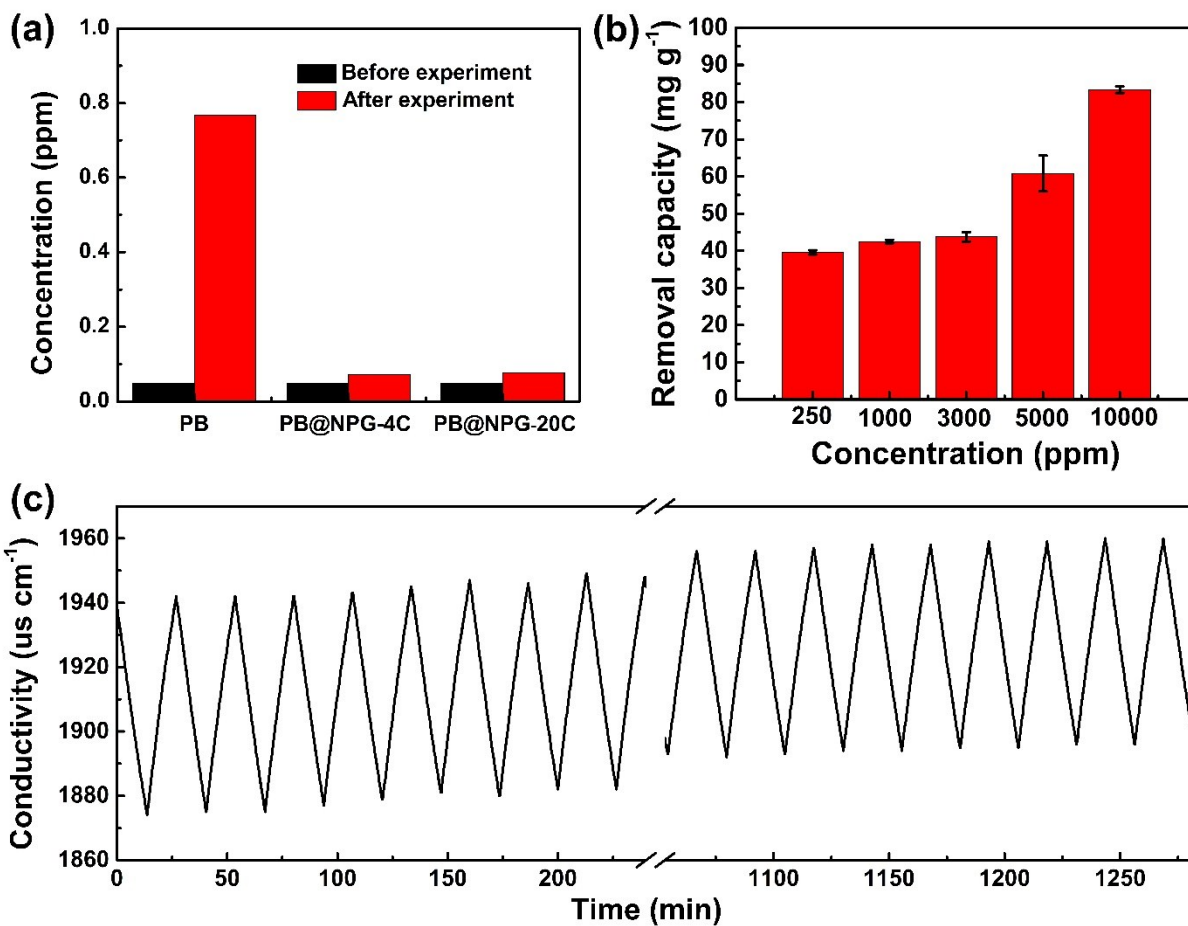


Figure S9. (a) The concentration of iron before and after cycling performance (From left to right: PB electrode after 100 cycles at 4C, PB@NPG electrode after 100 cycles at 4C, PB@NPG electrode after 600 cycles at 20C). (b) The removal capacity of PB@NPG electrodes at different concentration and 20C. (c) Electroadsorption behavior of PB@NPG electrode during cycling experiment at 1C.

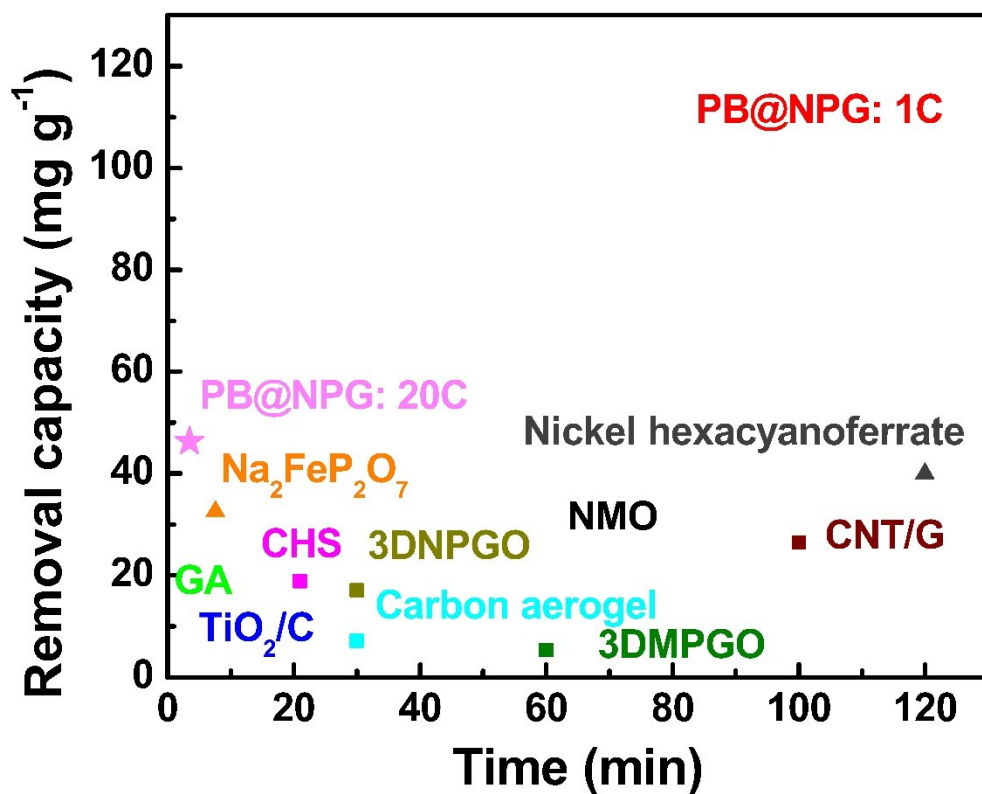


Figure S10. Comparison of the deionization performance and time consumption with other CDI methods.

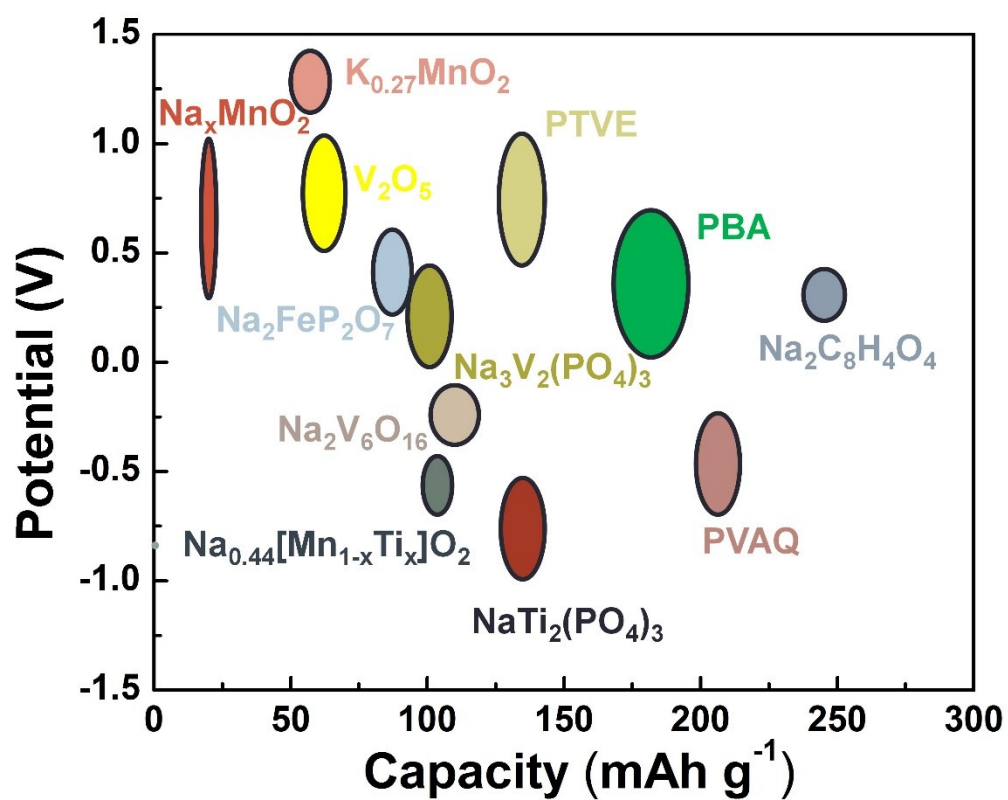


Figure S11. Reported materials that may be suitable for EDI. Report materials that may be suitable for EDI and the voltage versus capacity comparison in different aqueous batteries